

Research Article

DFT study of CO₂ activation on pristine and vacancy-containing 2D-GeC monolayers



Kamal Kumar^a, Abhishek Dhasmana^a, Nora H. de Leeuw^{b,c}, Jost Adam^{d,e},
 Abhishek K. Mishra^{a,*}

^a Department of Physics, Applied Science Cluster, School of Advanced Engineering, UPES, Dehradun 248007, India

^b Department of Chemistry, University of Leeds, Leeds LS2 9JT, UK

^c Department of Earth Sciences, Utrecht University, Utrecht 3584 CB, The Netherlands

^d Computational Materials and Photonics, Department of Electrical Engineering and Computer Science (FB 16) and Institute of Physics (FB 10), University of Kassel, Wilhelmshoher Allee 71, Kassel 34121, Germany

^e Center for Interdisciplinary Nanostructure Science and Technology, University of Kassel, Heinrich-Plett-Straße 40, Kassel 34132, Germany

ARTICLE INFO

Keywords:

2D GeC

DFT

CO₂ adsorption

Electrocatalysis

Defects

ABSTRACT

Designing a highly reactive adsorbent material for the catalytic conversion of carbon dioxide (CO₂) into valuable products to help ameliorate climate change and address the decreasing availability of fossil fuels is a widely explored application of two-dimensional (2D) nanomaterials. Herein, we present a 2D graphene-like monolayer (ML) of germanium (Ge) and carbon (C) atoms (2D GeC ML) for highly efficient CO₂ adsorption and activation. We have employed first-principles calculations based on the density functional theory (DFT) to investigate the adsorption behavior of CO₂ molecules at pristine GeC MLs and MLs containing defects/vacancies (C-vacancy V_C, Ge-vacancy V_{Ge}, and combined Ge- and C-vacancies V_{Ge/C}). We present a detailed description of the nature of the interaction and the mechanism of CO₂ conversion via in-depth projected densities of states, electronic band structures, charge density analysis, and Bader charge transfer analysis. The results show that CO₂ molecule weakly binds with the 2D GeC ML, with an adsorption energy (E_{ads}) of only -0.13 eV, rendering 2D GeC ML unsuitable for the reduction of CO₂. In contrast, CO₂ gas molecules show strong chemisorption on vacancy-defected GeC MLs with significant Bader charge transfer. The CO₂@GeC-V_{Ge} ML system displays a maximum E_{ads} of -4.46 eV, geometrical deformation, and a Bader charge transfer of -1.44 e⁻ to the CO₂ molecule. Thus, V_{Ge} is the most promising candidate among all considered GeC systems to enable the electrochemical CO₂ reduction reaction.

1. Introduction

The increasing concentration of anthropogenic carbon dioxide (CO₂) requires an immediate solution for its capture and conversion to various chemicals and fuels [1]. From a catalysis and surface chemistry perspective, two-dimensional (2D) nanomaterials provide various advantages such as a high surface-to-volume ratio and abundant active sites [2,3]. Their atomically thin structure facilitates efficient CO₂ adsorption due to maximum surface accessibility [2]. Additionally, the electronic properties of 2D materials can be easily tuned by various techniques such as doping and defect creation [4,5]. These techniques allow precise control over the catalytic activity of 2D materials, which makes them a promising candidate for CO₂ conversion reaction [6–9].

The presence of vacancies and defects in 2D materials is crucial for advancing their application in electrochemical CO₂ conversion [4]. Both intrinsic and engineered defects in 2D materials, such as vacan-

cies (monovacancies, divacancies), grain boundaries, and dopants, significantly change the chemical activity, adsorption sites, and local electronic band structure of 2D materials [10]. Vacancies create unsatisfied dangling bonds which bind with the CO₂ molecule and promote its activation by introducing various localized electronic states near the Fermi level [11]. Furthermore, these vacancies can lower the activation barrier of each reaction intermediate step [12]. These factors improve the overall selectivity and catalytic activity of 2D materials [12]. Vacancies may arise in 2D materials due to pressure and temperature variations, high-temperature annealing, and exposure to electron or ion beams, deviation from ideal stoichiometry, and lattice mismatch during the synthesis process [11–13]. Therefore, a study of various defects becomes essential for a more realistic experimental model of 2D materials [10,14].

Graphene is the most common and widely utilized group IVA-based 2D monolayer (ML) of carbon atoms arranged in a hexagonal honeycomb lattice [15]. More recently, scientific interest has also extended

* Corresponding author.

E-mail addresses: akmishra@ddn.upes.ac.in, mishra_ju@hotmail.com (A.K. Mishra).

to additional novel graphene-like hexagonal MLs from group 14 (IVA), such as germanene (2D counterpart of germanium) [16], silicene (2D counterpart of silicon) [17], stanene (2D counterpart of tin) [18] and plumbene (2D counterpart of lead) [19]. All of these MLs fall in the category of mono-elemental Xenics [20]. This novel category of 2D materials has established its irreplaceable position in the domain of sensors, energy storage, catalysis, spintronics, and optoelectronics [20]. The bi-elemental heterostructures of these MLs also exhibit unique physical and chemical properties [15]. For instance, recently, a 2D hexagonal structure of SiC has been designed by replacing half of the silicon atoms with carbon atoms and has been synthesized successfully as well [21]. Although the Si–C bond in 2D SiC ML exhibits sp^2 hybridization, silicon atoms of 2D SiC ML have more adsorption sites than carbon atoms. Thus, the presence of silicon atoms increases the overall activity of graphene [22].

2D bi-elemental ML of germanium carbide (GeC), also from the IVA group, exhibits wide band gap (E_g), which is advantageous in the design of new functional 2D MLs [21,23]. The 2D GeC ML combines germanene and graphene, in which the germanium and carbon atoms are arranged in a flat and hexagonal crystal lattice characterized by sp^2 -hybridization [24,25]. In contrast to buckled germanene, the GeC ML is stable only in a planar geometry [26]. Like other 2D materials, the electrical properties of 2D GeC ML depend on its thickness, which is determined by the number of layers [27,28]. Although GeC MLs have not yet been synthesized experimentally, amorphous or polycrystalline thin films of GeC have been obtained successfully through various methods. Li et al. prepared α -Ge_{1-x}C_x:H films from a mixed target of graphite and germanium using RF magnetron sputtering in a mixed atmosphere of H₂ and Ar gases and found that the optical band gap and electrical resistivity of the synthesized film increased with the H₂ gas flow rate [29]. Gupta et al. fabricated nano-crystalline Ge_xC_{1-x} thin films through radio frequency magnetron sputtering on a Si (100) substrate and confirmed structure, composition, and crystallinity using transmission electron and atomic force microscopy, Raman spectroscopy, and X-ray photoelectron spectroscopy (XPS). They detected a Raman signature for a local Ge–C mode near 530 cm⁻¹ at 350 °C for the fabricated thin films [30].

Different theoretical studies have been carried out to reveal the electrical, optical, mechanical, and magnetic properties of 2D GeC ML for various technological applications. Arellano et al. performed calculations based on the density functional theory (DFT) to study the adsorption of H₂ molecules on 2D GeC ML decorated by alkali metals (AM) and alkaline earth metals (AEM). Their study revealed that AEM weakly adsorbs on 2D GeC ML, while AM shows strong chemisorption. Compared to the nature of the adsorption of AMs and AEMs, the adsorption of H₂ on AEM falls in the category of physisorption [25]. Viquez et al. used DFT to study the interaction of diatomic gas molecules (NO, O₂, and N₂) with 2D GeC MLs decorated by noble metals (Cu, Ag, and Au). The calculated adsorption energies (E_{ads}) of O₂, NO, and N₂ gas molecules on pristine 2D GeC ML are 0.38, 0.40, and 0.16 eV, respectively. The decoration of the surface of 2D GeC ML by Au atoms promotes the charge transfer mechanism between gas molecules (O₂ and NO) and ML, and the E_{ads} of these molecules increase up to 1.00 and 1.35 eV, respectively. Similarly, the presence of the Au atom strengthens the binding of NO (1.23 eV) and O₂ (1.00 eV) molecules to the 2D GeC ML. The highest binding strength is obtained for NO gas molecules when 2D GeC MLs are decorated by Cu atoms [24]. Although the 2D GeC ML has been theoretically widely explored for various applications, including hydrogen storage and field effect transistors, its application in surface reactivity and CO₂ molecule adsorption and activation has not been explored extensively. This research gap motivated us to investigate its potential application in CO₂ activation. Therefore, in this paper, we systematically study CO₂ adsorption on pristine GeC and vacancy-containing GeC 2D monolayers through first-principles calculations based on density functional theory (DFT). The calculated projected densities of state (PDOS), electronic band structure (EBS), charge density analy-

sis, and Bader charge transfer confirm the nature and strength of the interaction.

2. Computational methodology and calculation details

DFT [31] calculations were carried out using the Quantum Espresso simulation package [32]. The exchange and correlation energies were modeled through the generalized gradient approximation (GGA) [33] along with Perdew–Burke–Ernzerhof (PBE) [34] functionals to model the interactions between ions and electrons [35]. The DFT–D3 method by Grimme was utilized to include weak Van der Waals interactions [36]. A plane wave basis with a well-converged kinetic energy cutoff of 44 Ry was used, and the Brillouin zone was sampled by $8 \times 8 \times 1$ k-mesh elements for the calculations of the electronic and adsorption properties of 2D GeC ML. To avoid interactions between the periodic images, we introduced a vacuum space of 15 Å perpendicular to the plane of the MLs. The energy and force criteria were set to 10^{-4} eV/Å and 10^{-3} eV, respectively, during the full relaxation of all geometrical structures. To improve the accuracy of the atomic orbital distributions of Ge and C atoms in our DFT calculations, we have chosen the tetrahedron method for electronic occupations with a dense mesh of $16 \times 16 \times 1$, while calculating their density-of-states.

The adsorption energy (E_{ads}) of CO₂ molecules was calculated using Eq. (1)

$$E_{\text{ads}} = E_{\text{GeC+CO}_2} - (E_{\text{GeC}} + E_{\text{CO}_2}), \quad (1)$$

where $E_{\text{GeC+CO}_2}$ and E_{GeC} are the total energies of 2D GeC MLs after and before CO₂ adsorption, respectively, while E_{CO_2} is the total energy of an isolated CO₂ molecule, simulated in a box.

3. Results and discussion

3.1. Structural and electronic properties

Pristine 2D GeC ML

The unit cell of 2D GeC ML consists of one Ge and one C atom, arranged in a planar hexagonal honeycomb lattice (see red ellipse in Fig. 1(a)). The equilibrium geometrical structure of 2D GeC ML is of the $P\bar{6}m2$ space group, where each Ge atom is attached to three C atoms. The optimized lattice parameters and bond lengths between the Ge and C atoms are 3.23 Å and 1.87 Å, respectively. The optimized cell parameter of our 2D GeC ML agrees well with the earlier reported values of Yang et al. (3.26 Å) [37], Xu et al. (3.23 Å) [38], Vu et al. (3.25 Å) [28] and Arellano et al. (3.26 Å) [25]. In the relaxed geometry, the Ge and C atoms lie in the same plane, and the calculated Ge–C–Ge (α) and C–Ge–C (β) bond angles are 119.99° and 120.01°, respectively. Moreover, sp^2 hybridization is present among both Ge–C–Ge and C–Ge–C arrangements. The dynamical stability of 2D GeC MLs was confirmed by Vu et al. [26]. Table 1 summarizes the relaxed cell parameters, bond lengths, bond angles, and calculated band gap, E_g , of GeC. The electronic configurations of the Ge and C atoms are $4s^2, 3d^{10}, 4p^2$ and $2s^2, 2p^2$, respectively. The calculated E_g of GeC is found to be 2.04 eV, indicating its semi-conducting nature. Our calculated value of the electronic band gap (E_g) is close to the earlier DFT calculated value of 2.07 eV by Yang et al. [37]. From the calculated electronic band structure (EBS) plot, shown in Fig. 1, it is clear that the top of the valence band (VB) and bottom of the conduction band (CB) lie at the same high symmetry point-K, indicating its direct bandgap semi-conducting nature. In order to understand the different orbital contributions to the EBS, we also performed the projected density of state calculations (PDOS), and from Fig. 1(c) it is clear that the major contributions to VB and CB arise from the Ge and C atom p-orbitals.

Vacancy defect-containing GeC MLs

In this section, we investigate the formation of vacancy defects in the 2D GeC ML. We investigated the formation of C-vacancy (V_C), Ge-

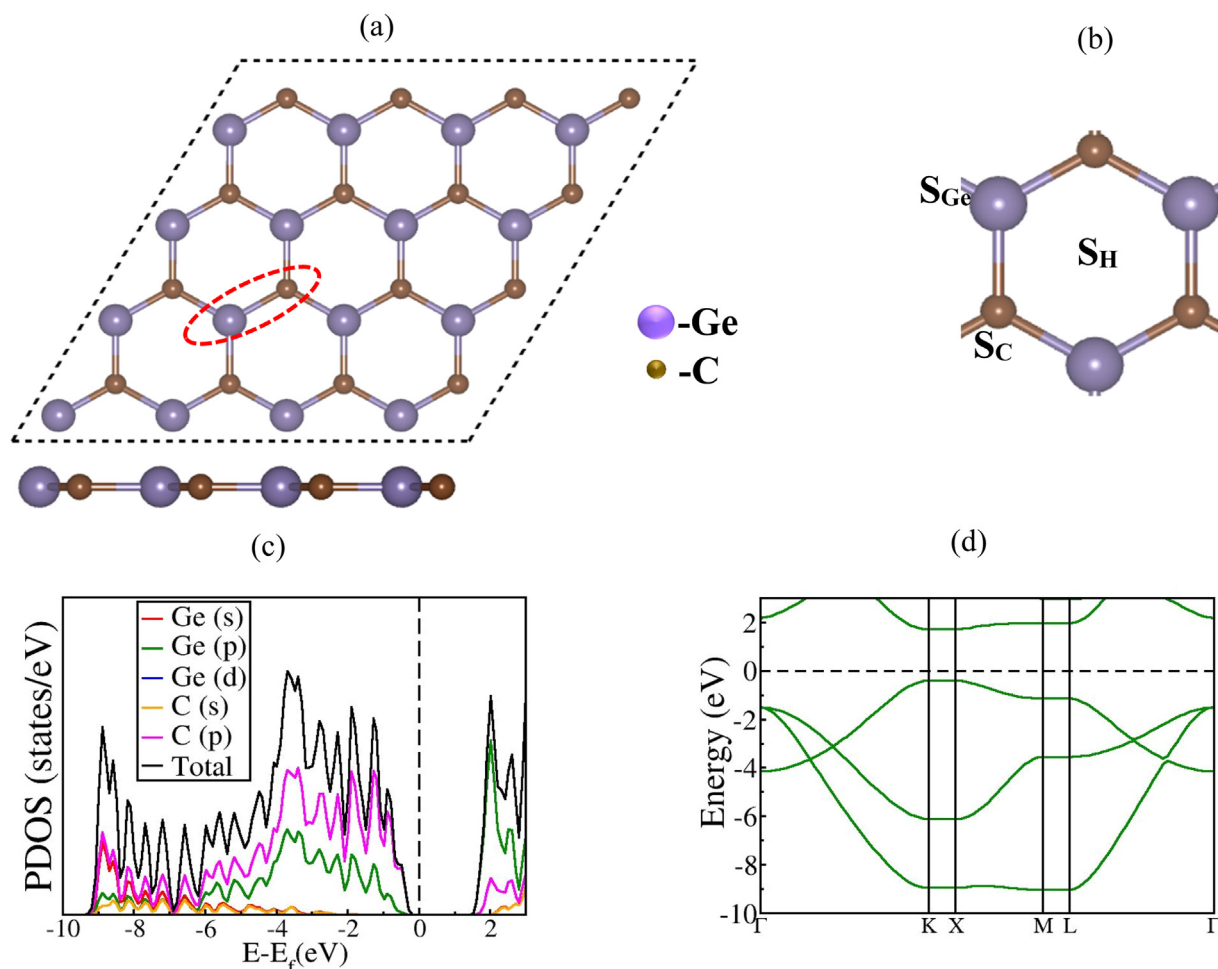


Fig. 1. (a) Top and side view of GeC ML, (b) active sites investigated for CO₂ adsorption, (c) PDOS, and (d) EBS of GeC unit cell. Violet and brown balls represent Ge and C atoms, respectively. The unit cell of GeC (marked with dotted red color) contains one Ge and one C atom. GeC has a planar structure with a direct band gap of 2.04 eV.

Table 1

Optimized cell parameters a , b (Å), bond length l (Å), bond angle α , β (°) of 2D GeC ML, and their comparison with earlier works.

	Our Study	Earlier DFT Works			
		Yang et al. [37]	Xu et al. [38]	Vu et al. [28]	Arellano et al. [25]
a	3.23	3.26	3.23	3.25	3.26
b	3.23	3.26	3.23	3.25	3.26
l (Ge-C)	1.87	1.88	1.86	1.87	–
α	119.99°	120°	–	–	–
β	120.01°	120°	–	–	–

vacancy (V_{Ge}), and combined Ge and C vacancies ($V_{\text{Ge/C}}$) GeC ML structures (Fig. 2), with the primary aim of understanding how these vacancies change the structural, electrical, and chemical characteristics of the 2D GeC MLs, which is crucial to understand CO₂ adsorption. For the investigation of vacancy formation, we employed a $4 \times 4 \times 1$ supercell of the 2D GeC ML.

The defect formation energy, E_{def} , was calculated as:

$$E_{\text{def}} = E_{\text{GeC}} - (E_{V_{\text{GeC}}} + E_{\text{X}}), \quad (2)$$

where E_{GeC} and $E_{V_{\text{GeC}}}$ represent the free energies of pristine and vacancy-containing GeC ML sheets, respectively, while E_{X} ($x = \text{Ge/C}$) is the energy of an isolated atom, removed from the pristine GeC ML sheet.

The calculated E_{def} for one C atom vacancy, using Eq. (2), is found to be -10.88 eV. The negative value indicates that the pristine sheet is sus-

ceptible to the formation of C vacancies. The formation of single C-atom vacancies in graphene was calculated by Lim et al. to be -7.70 eV using the same DFT GGA approach, which indicates that these vacancies are more susceptible in 2D GeC ML sheets compared to graphene MLs [39]. As a result of the introduction of this C atom vacancy, the Ge-C bond lengths surrounding the C-vacancy increase from 1.87 to 1.9 Å due to local distortions in the crystal lattice. As a result of the C-atom vacancy, the band gap disappears, and we note a shifting of states towards VB in the PDOS as well as in the EBS.

Next, we studied the Ge atom vacancy by removing one Ge atom from the 2D GeC ML sheet. As a result, the nearby Ge-C bond lengths contract by 2.13% due to the rearrangement of Ge and C atoms, decreasing their value to 1.83 Å from the initial 1.87 Å. The calculated E_{def} for one Ge atom vacancy was found to be -12.23 eV, indicating that a 2D GeC ML is more susceptible to the loss of Ge atoms. Monshi et al.

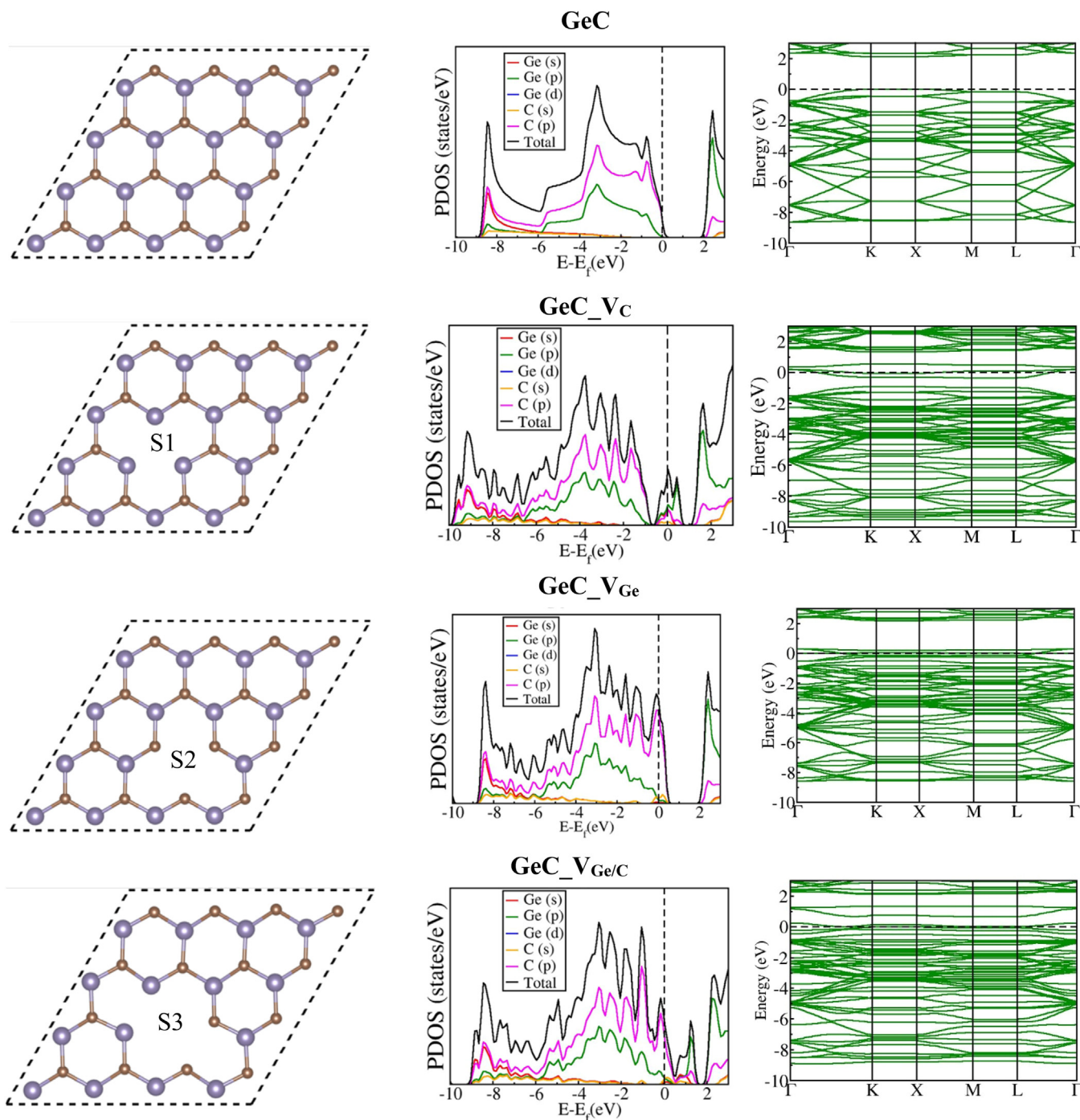


Fig. 2. Relaxed structure, PDOS and EBS of 2D GeC, GeC_{V_c}, GeC_{V_{Ge}} and GeC_{V_{Ge/C}} MLs. We have marked vacancy sites S1, S2, and S3 for V_c, V_{Ge} and V_{Ge/C} structures, respectively. 2D GeC ML transforms from semiconducting to metallic nature after C monovacancy and Ge/C divacancy.

studied the sensing performance of pristine and vacancy-containing germanene MLs, and reported a defect formation energy of -2.77 eV for a Ge vacancy in germanene [40] employing the same DFT-GGA approach. Thus, Ge vacancies are more favorable in 2D GeC MLs than in the pure germanene ML. The GeC_{V_{Ge}} ML shows an indirect band gap with an energy of 2.07 eV, where the CB minimum (CBM) and the VB maximum (VBM) values are found at the K and Γ high-symmetry points, respectively. Thus, V_c is metallic, while V_{Ge} is a semiconductor.

Creating a di-vacancy (combined Ge and C vacancies in the V_{Ge/C} system) expands the Ge and C atom bond separation up to 1.93 Å and reduces the band gap energy to 0.84 eV. The E_{def} of this di-vacancy

is -13.06 eV, the largest value among all considered vacancies. In summary, the vacancy probability in 2D GeC MLs decreases as: $V_{\text{Ge/C}} > V_{\text{Ge}} > V_{\text{c}}$. To study the impact of vacancy presence on the structure stability of 2D GeC ML, we performed phonon calculations at the Gamma point for GeC_{V_c}, GeC_{V_{Ge}} and GeC_{V_{Ge/C}} MLs. Notably, the absence of negative (imaginary) frequencies in all MLs indicates their dynamical stability. Thus, vacancy-induced defects do not lead to geometrical instabilities and 2D GeC ML maintains its dynamical robustness even in the presence of various vacancies. The calculated vibrational frequencies of defective GeC MLs are summarized in Table S1 of the supplementary information (SI).

Table 2

Calculated adsorption energy E_{ads} (eV), adsorption height h (Å), bond lengths l (Å), bond angle θ ($^\circ$), band gap E_g (eV), vibrational frequencies ν (cm^{-1}), and charge transfer Δq_{CO_2} of the most stable CO_2 configuration at pristine and vacancy-defected V-GeC MLs.

System	E_{ads}	h	l		θ	E_g	ν			Δq_{CO_2}
			Ge-C	C-O			ν_{as}	ν_{s}	ν_{b}	
Isolated CO_2	–	–	–	1.16, 1.16	180.00	–	2444	1367	604	–
GeC	–0.13	3.37	1.87	1.17, 1.17	179.96	2.09	2346	1318	643	–0.027
GeC_VC	–1.09	1.59	1.90	1.21, 1.32	125.04	1.09	1623	957	720	–0.354
GeC_VGe	–4.46	0.33	1.96	1.43, 1.40	104.87	1.39	724	692	455	–1.440
$\text{GeC}_V\text{Ge/C}$	–3.60	0.24	1.91	1.38, 1.30	110.91	0.98	1081	828	748	–1.154

In the PDOS of pristine 2D GeC, the major contribution in the entire VB and near E_F arises from Ge(p) and C(p) orbitals. But the presence of C vacancy in 2D GeC ML leads to augmentation of energy states at E_F attributed to the hybridization of C(p) and Ge(p) orbitals. As a result of this, the band gap of GeC_VC ML diminishes, which is also clear from EBS. While the Ge vacancy structure has nearly the same value of E_g as that of pristine 2D GeC ML, we observe some energy states at E_F due to the edge effect. Simultaneous creation of Ge and C vacancies leads to redistribution of orbitals at E_F due to hybridization of Ge(p) and C(p) orbitals.

3.2. CO_2 adsorption

Pristine GeC ML

In order to study the interaction of CO_2 molecules with 2D GeC MLs ($\text{CO}_2@GeC$), we identified three adsorption sites, denoted as S_{Ge} (above the Ge atom), S_{C} (above the C atom), and S_{H} (in the hollow portion of the hexagonal ring), as shown in Fig. 1. The CO_2 molecule was placed in two initial alignments: (i) perpendicular, and (ii) parallel to the plane of the 2D GeC ML. The relaxed geometries of all these $\text{CO}_2@GeC$ configurations are shown in Fig. S1 in the SI, whereas Table S2 contains all adsorption characteristics, including E_{ads} , adsorption height (h), bond angle (θ) of the CO_2 molecule, and the different bond lengths of CO_2 and Ge–C. We found that the alignments and positions of the CO_2 molecule significantly affect E_{ads} . E_{ads} of CO_2 in these configurations range between -0.06 to -0.13 eV. The calculated E_{ads} of CO_2 in horizontal alignments at S_{Ge} and S_{H} sites are -0.12 and -0.13 eV, respectively. While E_{ads} of CO_2 in horizontal alignment above S_{C} site is positive (0.17 eV). Thus, the adsorption process of CO_2 is endothermic and not thermodynamically unfavorable in this alignment. The E_{ads} of CO_2 at pristine 2D GeC ML in horizontal configurations are generally higher than those in vertical configurations. E_{ads} of CO_2 in vertical alignments at S_{C} , S_{Ge} and S_{H} sites are -0.06 , -0.08 and -0.09 eV, respectively. In all studied configurations, no dissociation of the CO_2 molecule is found during the adsorption process.

Fig. 3 shows the most stable configuration with the largest calculated value of E_{ads} of $\text{CO}_2@GeC$ to be -0.13 eV, with a 3.37 Å adsorption height at site S_{H} (Table 2), indicating S_{H} site to be most suitable for CO_2 adsorption on the pristine GeC ML. In this configuration, the CO_2 molecule remains linear after its interaction with the GeC ML. As expected, the Bader charge analysis reveals only a small charge transfer of $-0.027 e^-$ between GeC and the CO_2 molecule (Fig. 4(a)), where the CO_2 molecule acts as an electron acceptor. Comparison with earlier work shows that E_{ads} on GeC ML is higher than that on pristine germanene (-0.1 eV) [41]. While it is almost equal (-0.13 eV) to the E_{ads} of CO_2 at pristine silicene [42]. E_{ads} of CO_2 on pristine 2D GeC is 0.05 eV higher than that of analogous bi-elemental 2D ML SiC, which suggests marginally enhanced CO_2 capture ability of 2D GeC ML [22]. The interaction of CO_2 with GeC can be classified as a weak physisorption through Van der Waals interactions. The PDOS and EBS of $\text{CO}_2@GeC$ are shown in Fig. 3. From the PDOS, we observe that due to the weak interaction with the CO_2 molecule, the E_g of GeC remains almost the same (2.07 eV). A few new O atom p-orbital peaks are raised near the -6 and -10 eV energies in the PDOS, suggesting that the interaction

between GeC and CO_2 molecule occurs in the deep energy region of the VB. From EBS, we note that in pristine 2D GeC ML, the VBM was initially located near E_F , while after its interaction with the CO_2 molecule, there are minor shifts in the energy levels, and CBM comes close to E_F . Since the interaction was too weak, only a minor change (0.05 eV) was observed in E_g , and VBM and CBM remain at the same high symmetry point K. The obtained value of E_{ads} of $\text{CO}_2@GeC$ is less than the criteria set for practical applications (-0.14 eV) [42], rendering GeC unsuitable for practical adsorption, sensing, and conversion applications. Thus, further engineering is required to improve the activity of 2D GeC ML towards CO_2 activation.

Vacancy-containing 2D GeC MLs

In GeC_VC ML, one carbon atom was removed from the 2D GeC ML sheet, and this absence of C atom breaks the hexagonal ring and generates three dangling bonds (Fig. 2). The C-vacancy makes the 2D GeC ML more porous and generates a new active site for CO_2 interaction. Different vertical, horizontal, and tilted configurations of CO_2 molecules have therefore been studied at the defective site (marked S1 in Fig. 2) in the GeC_VC ML. The three most stable relaxed configurations of $\text{CO}_2@V_C$ are given in Fig. S2, and their adsorption parameters are summarized in Table S3. The most favorable configuration (configuration 1) was obtained by placing a linear CO_2 molecule horizontally near the S1 site, such that both O-atoms of CO_2 are above the Ge atoms of the GeC_VC ML and the structure was allowed to fully relax. Here, the calculated adsorption energy, E_{ads} , was found to be -1.09 eV (Fig. 3). The vertical height from the topmost surface atom of GeC_VC and the C atom of CO_2 after adsorption was 1.59 Å. The CO_2 molecule bends here to 125.04° and C–O bond lengths elongate to 1.21 and 1.32 Å from their initial values of 1.16 Å, indicating activation of the CO_2 molecule. This interaction in the GeC_VC system can be categorized as strong chemisorption, where the E_{ads} is 712% higher than that of a pristine GeC ML sheet. This strong chemisorption results in significant charge transfer of $-0.354 e^-$ (Fig. 4(b)). This strong binding directly affects the energy level distribution and atomic orbitals in the EBS and PDOS, as near the Fermi level, several new p-orbital peaks of O atom appear in the VB. Hence, the strong chemisorption of CO_2 disrupts the metallic character of the GeC_VC ML, leading to the opening of a direct band gap of 1.09 eV. As shown in Fig. 3, both the VBM and CBM are located near the high-symmetry point K, confirming the direct nature of the band gap.

Similar to a carbon atom vacancy, the absence of one Ge atom also results in three dangling bonds (unsaturated bonds of C atoms). For GeC_VGe ML, the highest value of E_{ads} for the CO_2 molecule was achieved (in configuration 2) when the CO_2 molecule was placed parallel to GeC_VGe ML at site S2 in such a fashion that both O atoms of CO_2 face the C atoms of V_{Ge} . In this arrangement, the CO_2 molecule bends to 104.87° , and both C–O bonds elongate to 1.43 and 1.40 Å. The calculated E_{ads} in this configuration were found to be -4.46 eV (Fig. 3), which is 3.38 eV higher than the E_{ads} for the $\text{CO}_2@GeC_V\text{C}$ system. As expected, a high amount of Bader charge ($-1.440 e^-$) is transferred between the CO_2 molecule and the GeC_VGe ML, confirming the oxidation of V_{Ge} (see Fig. 4(c)). This strong binding and bending in the linear CO_2 molecule confirm chemisorption in the GeC_VGe system. The E_g

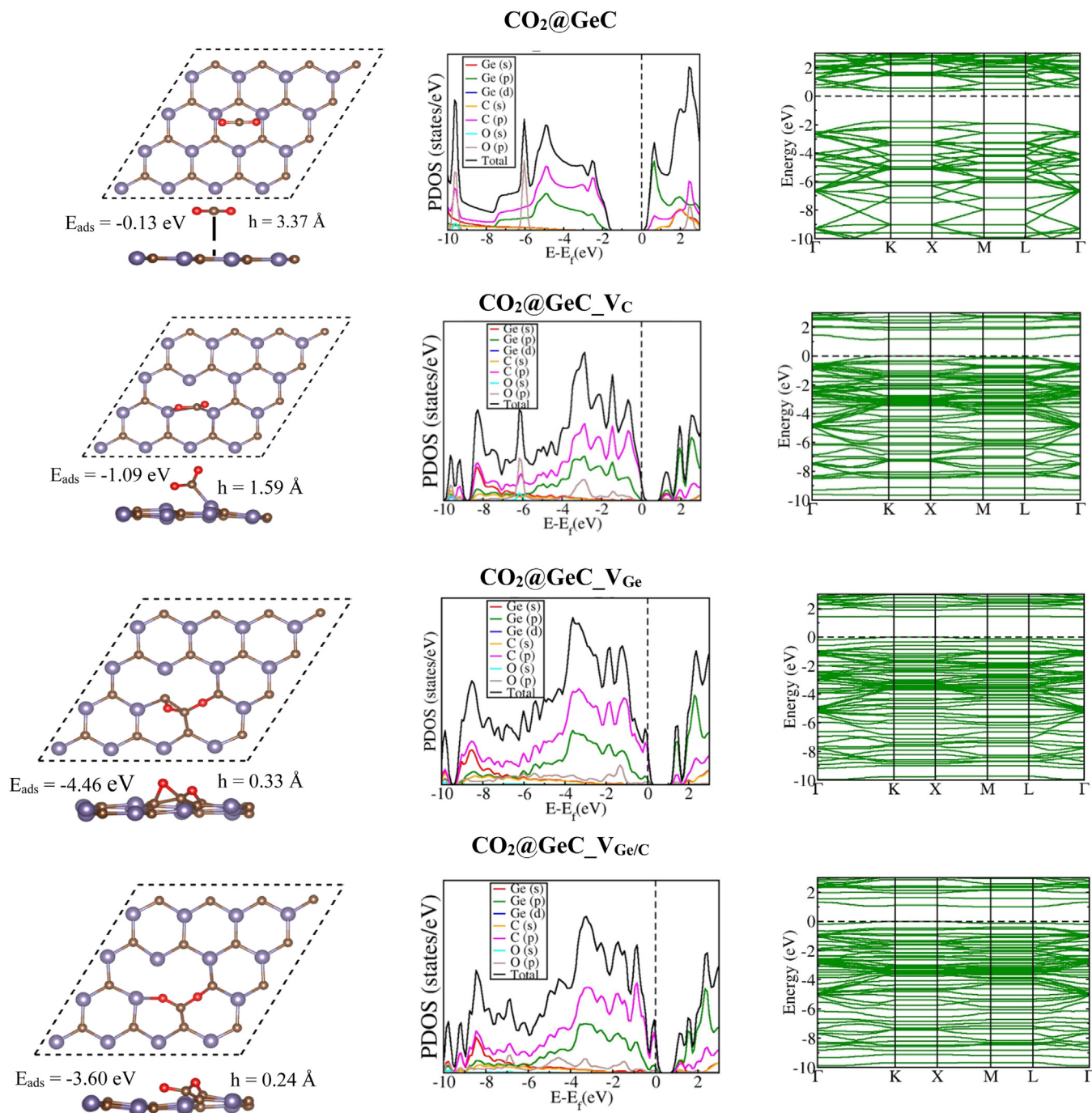


Fig. 3. Top and side view of relaxed geometries, PDOS, and EBS of 2D GeC, GeC_{Vc}, GeC_{VGe}, and GeC_{VGe/C} MLs after CO₂ adsorption. GeC_{Vc}, GeC_{VGe} and GeC_{VGe/C} MLs activate linear CO₂ molecules, and the maximum energy of CO₂ is achieved at GeC_{VGe} ML.

was found to decrease from its value of 2.07 to 1.39 eV, and the CO₂ molecule vertical absorption height was 0.33 Å. The PDOS analysis indicates the uniform contribution of the CO₂ molecule's O atom p-orbitals in the entire VB. The band structure and projected density of states (PDOS) reveal the emergence of new states around 1.4 eV, originating from the p-orbital of the carbon atom in the CO₂ molecule. This results in a reduction of the band gap from 2.07 to 1.39 eV. The relaxed structures and adsorption characteristics of all investigated CO₂ molecule configurations at the GeC_{VGe} ML are shown in Fig. S3 and Table S4, respectively.

For the di-vacancy 2D GeC ML (GeC_{VGe/C}), we identified site S3 (Fig. 2) to explore its interaction with the CO₂ molecule. Similar to

the other studied vacancies, we found that after full relaxation, the CO₂ molecule chemically gets adsorbed on GeC_{VGe/C} ML with E_{ads} of -3.60 eV (in configuration 3), when one O atom of CO₂ faces the C atom of V_{Ge/C}, and another O atom is near site S3 in horizontal alignment. This E_{ads} is higher than that in CO₂@ GeC_{Vc} ML by an amount of 2.52 eV, but smaller than in CO₂@ GeC_{VGe} ML by an amount of 0.86 eV. Not only E_{ads} but also all remaining adsorption parameters (C–O and Ge–C bond lengths, bond angle of CO₂ molecule, and charge transfer) fall between those of the GeC_{Vc} and GeC_{VGe} MLs. The CO₂ molecule bends to $\sim 111^\circ$ and C–O bonds elongate to 1.38 and 1.30 Å. The CO₂ molecule gains a 1.154 e[−] negative charge (Fig. 4(d)), and the band gap of the system changes to 0.98 eV from its initial value of 0.84 eV. Fig. S4 and

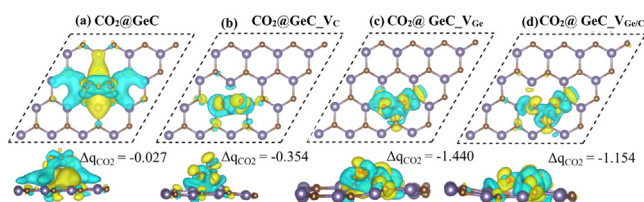


Fig. 4. Charge density difference plots of most stable configurations of the CO₂ molecule at (a) GeC, (b) GeC_V_c, (c) GeC_V_{Ge}, and (d) GeC_V_{Ge/C} (yellow and blue colors represent positive and negative charges, respectively). Maximum charge transfer (−1.440 e[−]) takes place between the CO₂ molecule and 2D GeC_V_{Ge} ML.

Table S5 in the supplementary information show the post-adsorption geometries and parameters of the different CO₂@V_{GeC}-GeC system configurations. Table 2 contains all adsorption parameters of the most stable configurations of pristine as well as vacancy-defected 2D GeC MLs.

To further investigate the activation of CO₂, we calculated vibrational frequencies of adsorbed CO₂ molecules on different 2D GeC MLs and compared them with those of an isolated CO₂ molecule. We note that in pristine 2D GeC ML, as the interaction was a weak physisorption, where the molecule remained linear after interaction, a very weak change in frequencies is noted. Whereas, strong chemisorption in vacancy-defected GeC MLs results in a large change in CO₂ molecule vibrational frequencies. After adsorption on pristine 2D GeC ML, symmetric (ν_s) and asymmetric (ν_{as}) C–O vibrational modes of CO₂ suffer a very small red shift of 49 and 98 cm^{−1} as its changes to 1318 and 2346 from its value of 1367 and 2444 cm^{−1} respectively, while bending mode (ν_b) show slight blue shift and changes its value to 643 cm^{−1} from its initial value of 604 cm^{−1}. In defected 2D GeC monolayers, strong chemisorption of the CO₂ molecule at vacancy sites leads to significant structural distortions, including molecular bending and elongation of the C–O bonds. These changes result in pronounced red shifts in both the symmetric (ν_s) and asymmetric (ν_{as}) vibrational modes of CO₂, with the largest shift observed in the GeC_V_{Ge} monolayer, where ν_s and ν_{as} shift to 692 and 724 cm^{−1}, respectively. This is attributed to the elongation of the C–O bonds from their initial length of 1.16 to 1.43 and 1.40 Å. Additionally, the bending mode (ν_b) shifts from its initial value of 604 to 455 cm^{−1}, corresponding to the loss of molecular linearity and the formation of a bent geometry (~105°) upon binding to the Ge-vacancy site. These changes in vibrational modes reflect a high degree of CO₂ activation, suggesting that such defected GeC systems may serve as promising platforms for further reactions, such as CO₂ hydrogenation or the reverse water–gas shift reaction after getting converted into CO or other value-added products.

4. Conclusion

We have employed DFT calculations to investigate the adsorption behaviour of CO₂ molecules at pristine and vacancy-containing GeC MLs. The strength of interaction and nature of the adsorption are explored through PDOS, EBS, charge density difference analyses, Bader charge transfer, and phonon calculations. The E_{ads} calculations suggest that CO₂ molecules prefer to adsorb physically on perfect GeC MLs with a small E_{ads} of −0.13 eV. We found that the presence of C, Ge, and Ge/C vacancies is energetically favorable. The interaction of CO₂ with all three vacancy-containing MLs (GeC_V_c, GeC_V_{Ge}, and GeC_V_{Ge/C}) can be categorized as strong chemisorption from the high E_{ads} (−1.09, −4.46, and −3.60 eV, respectively) and geometrical deformation of the CO₂ molecule as a result of interaction with MLs. GeC_V_{Ge} MLs are found to be most favorable for the further catalytic conversion of CO₂, shown by the largest CO₂ adsorption capacity and maximum amount of Bader charge transfer of −1.44 e[−].

Declaration of Competing Interest

The authors declare that they have no known competing financial interests or personal relationships that could have appeared to influence the work reported in this paper.

CRediT authorship contribution statement

Kamal Kumar: Writing – original draft, Investigation, Validation, Conceptualization, Visualization, Formal analysis. **Abhishek Dhasmana:** Formal analysis, Investigation. **Nora H. de Leeuw:** Resources, Software, Writing – review & editing. **Jost Adam:** Resources, Software, Writing – review & editing. **Abhishek K. Mishra:** Writing – review & editing, Software, Methodology, Conceptualization, Supervision, Project administration, Funding acquisition, Validation, Resources, Investigation.

Acknowledgements

Prof. Abhishek K. Mishra (AKM) acknowledges the Science and Engineering Research Board (SERB) for a state university research excellence (SURE) grant (SUR/2022/004935). Via our membership of the UK's HEC Materials Chemistry Consortium, which is funded by EPSRC (EP/X035859), we also acknowledge the use of the ARCHER2 UK National Supercomputing Service (<https://www.archer2.ac.uk>). This research work was conducted with the financial support, provided by UPES, Dehradun, India.

Supplementary materials

Supplementary material associated with this article can be found, in the online version, at [doi:10.1016/j.chphma.2025.06.002](https://doi.org/10.1016/j.chphma.2025.06.002).

References

- [1] M.D. Garba, M. Usman, S. Khan, F. Shehzad, A. Galadima, M.F. Ehsan, M. Humayun, CO₂ towards fuels: A review of catalytic conversion of carbon dioxide to hydrocarbons, *J. Environ. Chem. Eng.* 9 (2021) 104756, doi:10.1016/j.jece.2020.104756.
- [2] D. Deng, K.S. Novoselov, Q. Fu, N. Zheng, Z. Tian, X. Bao, Catalysis with two-dimensional materials and their heterostructures, *Nat. Nanotechnol.* 11 (2016) 218–230, doi:10.1038/nnano.2015.340.
- [3] K. Kumar, J. Xu, G. Wu, A. Verma, A.K. Mishra, L. Gao, S. Ogata, Recent trends and progress in molecular dynamics simulations of 2D materials for tribological applications: An extensive review, *Arch. Computat. Method. Eng.* (2025) 1–23, doi:10.1007/s11831-025-10257-0.
- [4] E.J. Jelmy, N. Thomas, D.T. Mathew, J. Louis, N.T. Padmanabhan, V. Kumaravel, H. John, Impact of structure, doping and defect-engineering in 2D materials on CO₂ capture and conversion, *React. Chem. Eng.* 6 (2021) 1701–1738, doi:10.1039/D1RE00214G.
- [5] L. Yu, F. Li, J. Huang, B.G. Sumpter, W.E. Mustain, Z. Chen, Double-atom catalysts featuring inverse sandwich structure for CO₂ reduction reaction: A synergetic first-principles and machine learning investigation, *ACS Catal.* 13 (2023) 9616–9628, doi:10.1021/acscatal.3c01584.
- [6] N. Martin, N. Tagmatarchis, Q.H. Wang, X. Zhang, Chemical functionalization of 2D materials, *Chem. Eur. J.* 26 (2020) 6292–6295, doi:10.1002/chem.202001304.
- [7] F. Lee, M. Tripathi, R.S. Salas, S.P. Ogilvie, A.A. Graf, I. Jurewicz, A.B. Dalton, Localised strain and doping of 2D materials, *Nanoscale* 15 (2023) 7227–7248, doi:10.1039/D2NR07252A.
- [8] J. Su, L. Yu, B. Han, F. Li, Z. Chen, X.C. Zeng, Enhanced CO₂ reduction on a Cu-decorated single-atom catalyst via an inverse sandwich M-graphene-Cu structure, *J. Phys. Chem. Lett.* 15 (2024) 8600–8607, doi:10.1021/acs.jpclett.4c01858.
- [9] K. Kumar, N.H. de Leeuw, J. Adam, A.K. Mishra, Mechanistic insights into CO₂ activation on pristine, vacancy-containing and doped goldene: A single-atom layer of gold, *Phys. Chem. Chem. Phys.* 26 (2024) 29420–29431, doi:10.1039/d4cp03087g.
- [10] T. Sun, G. Zhang, D. Xu, X. Lian, H. Li, W. Chen, C. Su, Defect chemistry in 2D materials for electrocatalysis, *Mater. Today Energy* 12 (2019) 215–238, doi:10.1016/j.mtener.2019.01.004.
- [11] H. Zhang, R. Lv, Defect engineering of two-dimensional materials for efficient electrocatalysis, *J. Materiom.* 4 (2018) 95–107, doi:10.1016/j.jmat.2018.02.006.
- [12] L. Zhao, B. Wang, R. Wang, A critical review on new and efficient 2D materials for catalysis, *Adv. Mater. Interfaces* 9 (2022) 2200771, doi:10.1002/admi.202200771.
- [13] R.C. Walker, T. Shi, E.C. Silva, I. Jovanovic, J.A. Robinson, Radiation effects on two-dimensional materials, *Phys. Status Solid. A* 213 (2016) 3065–3077, doi:10.1002/pssa.201600395.
- [14] K. Kumar, A. Dhasmana, S. Mishra, R. Sharma, N.H. de Leeuw, J. Adam, A.K. Mishra, Defect-mediated CO₂ activation at two-dimensional MgO monolayers: A DFT study, *Mater. Today Commun.* 46 (2025) 112907, doi:10.1016/j.mtcomm.2025.112907.

- [15] J.C. Garcia, D.B. de Lima, L.V.C. Assali, J.F. Justo, Group-IV graphene and graphane-like nanosheets, *J. Phys. Chem. C* 115 (2011) 13242–13246, doi:10.1021/jp203657w.
- [16] N.M. Al-Shareefi, A.A. Al-Jobory, H.I. Abbood, Germanene-GaAs as super media for gas sensor, *IOP Conf. Ser. Mater. Sci. Eng.* 454 (2018) 012153, doi:10.1088/1757-899X/454/1/012153.
- [17] A. Molle, C. Grazianetti, L. Tao, D. Taneja, M.H. Alam, D. Akinwande, Silicene, silicene derivatives, and their device applications, *Chem. Soc. Rev.* 47 (2018) 6370–6387, doi:10.1039/C8CS00338F.
- [18] G. Gao, Y. Jiao, F. Ma, Y. Jiao, L. Kou, E. Waclawik, A. Du, Versatile two-dimensional stanene-based membrane for hydrogen purification, *Int. J. Hydrog. Energy* 42 (2017) 5577–5583, doi:10.1016/j.ijhydene.2016.07.119.
- [19] Vivek, M. Sharma, R. Sharma, Plumbene: A next generation hydrogen storage medium, *Int. J. Hydrog. Energy* 46 (2021) 33197–33205, doi:10.1016/j.ijhydene.2021.07.159.
- [20] Z. Liu, J. Liu, P. Yin, Y. Ge, O.A. Al-Hartomy, A. Al-Ghamdi, S. Wagesh, Y. Tang, H. Zhang, 2D Xenos: Optical and optoelectronic properties and applications in photonic devices, *Adv. Funct. Mater.* 32 (2022) 220650, doi:10.1002/adfm.202206507.
- [21] L.B. Drissi, K. Sadki, M.H. Kourra, Mechanical response of SiC sheet under strain, *Mater. Chem. Phys.* 201 (2017) 199–206, doi:10.1016/j.matchemphys.2017.08.016.
- [22] Z. Zhao, Y. Yong, Q. Zhou, Gas-sensing properties of the SiC monolayer and bilayer: A density functional theory study, *ACS Omega* 5 (2020) 12364–12373, doi:10.1021/acsomega.0c01084.
- [23] L.B. Drissi, F.Z. Ramadan, N.B.J. Kanga, Fluorination-control of electronic and magnetic properties in GeC-hybrid, *Chem. Phys. Lett.* 659 (2016) 148–153, doi:10.1016/j.cplett.2016.07.017.
- [24] A.L. Marcos-Viquez, L.G. Arellano, Á. Miranda, Adsorption of diatomic gas molecules on transition-metal-decorated GeC monolayers, *J. Mater. Sci.* 57 (2022) 8455–8463, doi:10.1007/s10853-021-06827-9.
- [25] L.G. Arellano, F. De Santiago, Á. Miranda, Ab initio study of hydrogen storage on metal-decorated GeC monolayers, *Int. J. Hydrog. Energy* 46 (2021) 29261–29271, doi:10.1016/j.ijhydene.2021.04.135.
- [26] T.V. Vu, N.T.T. Anh, D.M. Hoat, Electronic, optical and photocatalytic properties of fully hydrogenated GeC monolayer, *Phys. E: Low-Dimens. Syst. Nanostruct.* 117 (2020) 113857, doi:10.1016/j.physe.2019.113857.
- [27] Z. Sohbatazadeh, H.A. Eivari, D.V. Fakhrabad, Formation energy and some mechanical properties of hydrogenated hexagonal monolayer of GeC, *Phys. B Condens. Matter* 547 (2018) 88–91, doi:10.1016/j.physb.2018.08.009.
- [28] T.V. Vu, N.T.T. Anh, D.P. Tran, Surface functionalization of GeC monolayer with F and Cl: electronic and optical properties, *Superlatt. Microstruct.* 137 (2020) 106359, doi:10.1016/j.spmi.2019.106359.
- [29] Y. Li, C. Li, Z. Xu, Z. Liu, Effects of hydrogen incorporation on structural, optical and electrical properties of germanium carbon films prepared with RF magnetron co-sputtering, *J. Alloy. Compd.* 694 (2017) 647–652, doi:10.1016/j.jallcom.2016.10.046.
- [30] N. Gupta, B.P. Veettil, H. Xia, Synthesis of nano-crystalline germanium carbide using radio frequency magnetron sputtering, *Thin Solid Films*. 592 (2015) 162–166, doi:10.1016/j.tsf.2015.09.014.
- [31] W. Kohn, Density functional theory for systems of very many atoms, *Int. J. Quant. Chem.* 56 (1995) 229–232, doi:10.1002/qua.560560407.
- [32] P. Giannozzi, O. Andreussi, T. Brumme, O. Bunau, M. Buongiorno Nardelli, M. Calandra, R. Car, C. Cavazzoni, D. Ceresoli, M. Cococcioni, N. Colonna, I. Carnimeo, A. Dal Corso, S. de Gironcoli, P. Delugas, R.A. DiStasio Jr, A. Ferretti, A. Floris, G. Fratesi, G. Fugallo, R. Gebauer, U. Gerstmann, F. Giustino, T. Gorni, J. Jia, M. Kawamura, H.-Y. Ko, A. Kokalj, E. Küçükbenli, M. Lazzeri, M. Marsili, N. Marzari, F. Mauri, N.L. Nguyen, H.-V. Nguyen, A. Otero-de-la-Roza, L. Paulatto, S. Poncè, D. Rocca, R. Sabatini, B. Santra, M. Schlipf, A.P. Seitsonen, A. Smogunov, I. Timrov, T. Thonhauser, P. Umari, N. Vast, X. Wu, S. Baroni, Advanced capabilities for materials modelling with Quantum ESPRESSO, *J. Phys.: Condens. Matter* 29 (2017) 465901, doi:10.1088/1361-648X/aa8f79.
- [33] J.P. Perdew, K. Burke, M. Ernzerhof, Generalized gradient approximation made simple, *Phys. Rev. Lett.* 77 (1996) 3865–3868, doi:10.1103/PhysRevLett.77.3865.
- [34] Z. Wan, Q. De Wang, D. Liu, J. Liang, Effectively improving the accuracy of PBE functional in calculating the solid band gap via machine learning, *Comput. Mater. Sci.* 198 (2021) 110699, doi:10.1016/j.commatsci.2021.110699.
- [35] P.E. Blochl, Projector augmented – wave method, *Phys. Rev. B* 50 (1994) 17953–17979, doi:10.1103/PhysRevB.50.17953.
- [36] J. Moellmann, S. Grimme, DFT-D3 study of some molecular crystals, *J. Phys. Chem. C* 118 (2014) 7615–7621, doi:10.1021/jp501237c.
- [37] J. Yang, C. Chen, J. Zhang, High-performance p-type 2D FET based on Monolayer GeC with high hole mobility: A DFT-NEGF study, *Adv. Electron. Mater.* 8 (2022) 2200388, doi:10.1002/aelm.202200388.
- [38] Z. Xu, Y. Li, Z. Liu, S.F. Liu, Electronic and magnetic behaviors of B, N, and 3d transition metal substitutions in germanium carbide monolayer, *J. Magn. Mater.* 451 (2018) 799–807, doi:10.1016/j.jmmm.2017.11.026.
- [39] D.H. Lim, A.S. Negreira, J. Wilcox, DFT studies on the interaction of defective graphene-supported Fe and Al nanoparticles, *J. Phys. Chem. C* 115 (2011) 8961–8970, doi:10.1021/jp2012914.
- [40] M.M. Monshi, S.M. Aghaei, I. Calizo, Doping and defect-induced germanene: A superior media for sensing H₂S, SO₂ and CO₂ gas molecules, *Surf. Sci.* 665 (2017) 96–102, doi:10.1016/j.susc.2017.08.012.
- [41] W. Xia, W. Hu, Z. Li, J. Yang, A first-principles study of gas adsorption on germanene, *Phys. Chem. Chem. Phys.* 16 (2014) 22495, doi:10.1039/c4cp03292f.
- [42] J. Zhu, A. Chronoes, U. Schwingenschlög, CO₂ capture by Li-functionalized silicene, *Phys. Status Solidi. RRL* 10 (2016) 458–461, doi:10.1002/pssr.201600102.